Title

The adhesion capability of *S. aureus* cells is heterogeneously distributed over the cell envelope

Authors

Christian Spengler[1], Bernhard A. Glatz[2], Erik Maikranz[3], Markus Bischoff[4], Michael Andreas Klatt[5†], Ludger Santen[3], Andreas Fery[2,6], Karin Jacobs[1,7]*

Affiliations

[1]: Experimental Physics, Saarland University, Center for Biophysics, 66123 Saarbrücken, Germany

[2]: Institute of Physical Chemistry and Physics of Polymers, Leibniz Institute of Polymer Research, 01069 Dresden, Germany

[3]: Theoretical Physics, Saarland University, Center for Biophysics, 66123 Saarbrücken, Germany

[4]: Institute of Medical Microbiology and Hygiene, Saarland University, Center for Biophysics, 66421 Homburg/Saar, Germany

[5]: Department of Physics, Princeton University, Jadwin Hall, Princeton, NJ 08544-0001, USA

[†]: Present addresses: Institute of Theoretical Physics, Friedrich-Alexander-Universität Erlangen-Nürnberg (FAU), 91058 Erlangen, Germany, and Department of Experimental Physics, Saarland University, 66123 Saarbrücken, Germany

[6]: Physical Chemistry of Polymer Materials, Technical University Dresden, 01062 Dresden, Germany

[7]: Max Planck School Matter to Life, 69120 Heidelberg, Germany

*: E-mail: k.jacobs@physik.uni-saarland.de; Fax: +49 (0)681 302 71700;
Tel: +49 (0)681 302 71777

Abstract

Understanding and controlling microbial adhesion is an important biomedical problem. However, many properties of the adhesion process of bacteria are still unknown, for example the distribution of adhesive strength over the cell wall. While a patchy colloid model for adhesion has been developed recently for Gram-negative *Escherichia coli* cells, a comparable model for Gram-positive cells is not known. Here, we use single-cell force spectroscopy to measure the adhesion of *Staphylococcus aureus* at different positions on tailored surfaces. We find a heterogenous distribution of the adhesion forces with varying degrees of intensity. By comparing these results to simulations, we obtain the distribution of adhesive strength on the cell wall: The cells have several distinct spots of high adhesion capability, similar to the patchy colloid model. We discuss implications of our results for the development of new materials and the design and analysis of future studies.

Introduction

Infections caused by bacterial biofilms are a major healthcare problem (1-3). These biofilms can be found both on natural surfaces, e. g. in the nasal (4) and oral (5) cavity, as well as on artificial surfaces, such as the exterior of prostheses, catheters and other medical devices (6-9). In this context, *Staphylococcus aureus* (*S. aureus*) is an important human pathogen (10, 11), which is capable of forming biofilms with increased resistance to antibiotic treatment (12) and the body's own immune system (13). Consequently, *S. aureus* can cause various diseases (14), such as superficial skin disease, sepsis, endocarditis and pneumonia (10). Since the formation of a biofilm begins with the attachment of single bacterial cells, understanding and controlling bacterial adhesion to solid surfaces is an urgent challenge in biomedical research.

Previous studies demonstrated that *S. aureus* cells adhere by tethering cell wall macromolecules, the number of which varies greatly depending on the properties of the underlying substrate (15, 16). The number and properties of individual tethering molecules define the adhesive strength (17), and by length fluctuations, the molecules can overcome certain degrees of surface roughness (18). For the secretion and deposition of adhesins on the *S. aureus* cell wall, different mechanisms have been unraveled (19). In particular, it has been shown that protein A is secreted very selectively near the septum and then built into the cell wall (20). In another study, however, accumulation of protein A was also observed in additional areas of the cell wall and differences in the frequency and density of these clusters

depending on the growth phase could be detected (21). The same study also observed cluster formation for clumping factor A (ClfA), whose size, but not the frequency, was growth phase-dependent (21). Atomic force microscopy (AFM) has been used in many studies to find specific interactions between functionalized probes and certain proteins at the cell wall (22-26). While in these studies, ClfA and B as well as the fibronectin-binding protein A (FnbpA) have not been found to be distributed in distinct clusters (22-24), it has been found that the collagen-binding protein (Cna) in *S. aureus* (25) and Serine-aspartate repeat-containing protein G (SdrG) in *Staphylococcus epidermis* (26) show a cluster-like distribution.

However, the question of how the overall adhesion capability of *S. aureus* or other Gram-positive cells is distributed over the cell surface has not yet been answered. For Gram-negative *Escherichia coli* (*E. coli*) cells, it has been found recently that this species adheres to glass surfaces by adhesive patches on their cell wall, and that the number of patches defines the adhesive strength (27). However, Gram-positive *S. aureus* cells have a very different cell wall composition and cell division behavior than *E. coli* cells, and it has been shown that the size of the contact area between cell and surface does not correlate with its adhesive strength. In particular it has been shown that the size of the contact area of different strains is largely comparable while they may differ vastly in terms of adhesive strengths (17).

In this study, we performed single-cell force spectroscopy (SCFS) on a periodically structured surface to directly measure the adhesion of different positions of the *S. aureus* cell wall to an unconditioned abiotic surface. We used a PDSM substrate with a symmetrical, periodic surface topography with a wavelength in the size range slightly above the cell diameter. The surfaces were formed by a controlled wrinkling process that allowed patterning in a scalable fashion and has found applications in various studies (28-30). With these substrates and the precise control of the lateral distance between several consecutive force-distance curves on the substrate's surface, we were able to probe different parts of the cell envelope in terms of their adhesion capability. Our experiments show that the adhesive strength at a given position is quite robust over the course of several measurements but can vary greatly for different cell wall positions depending on the individual cell.

By reproducing these experimental results with Monte Carlo (MC) simulations according to a recent model of adhesion (15), we show that the adhesion capability of *S. aureus* is driven by adhesins organized in distinct patches of various number over the cell envelope.

These results are important for the fabrication of new materials and the design of more precise models to describe bacterial adhesion.

Results

Wrinkled PDMS surfaces are a periodic, symmetrical, and therefore suitable substrate

Since AFM-based force-distance curves can only be recorded by a vertical movement of a bacterial probe, surfaces providing flanks with slopes of suitable absolute values in positive and negative direction are required to measure the adhesion at different positions of the cell surface by SCFS (see Fig. 1a). Moreover, a substrate with a continuous transition from positive to negative local slopes would allow to probe not only two points, but also intermediate positions (see Fig. 1b). These requirements can be met by wrinkled PDMS surfaces, which are shown in Figure 1c and 1d (28, 29).

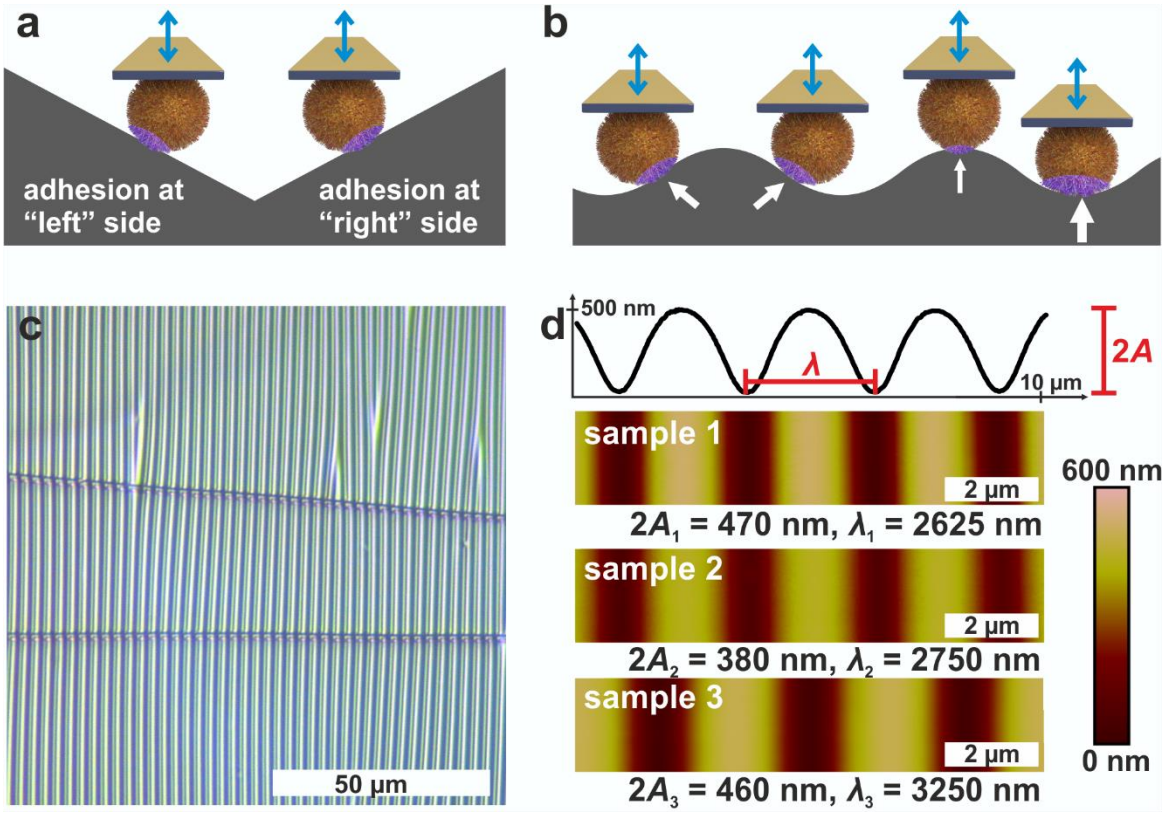

Fig. 1. Measuring principle on wrinkled PDMS. a) Probing both sides of a cell on a substrate with negative and positive slope. b) Possibility to continuously probe different positions (indicated by arrows) of a cell on a substrate with a symmetric structure of changing local slope. c) Optical micrograph of wrinkled PDMS. d) AFM images of the wrinkled PDMS surfaces. For sample 1, a cross-section of the surface is shown to define the structure's amplitude A and wavelength λ, which are displayed for every sample surface.

The optical micrograph shows that the wrinkled PDMS substrate has quite a homogeneous wrinkle structure over a large area, which is only rarely disrupted by cracks in the material (Fig. 1c). To characterize the surface topography in all dimensions, the wrinkled PDMS was analyzed via topographical AFM (Fig. 1d). For our experiments, we used three different PDMS samples, which were produced with slightly varying parameters. Figure 1 d shows AFM images of all samples. In addition, a scan line recorded on sample 1 is depicted, in which the specific wrinkling parameters, wavelength λ and amplitude *A*, are defined. All samples have a very homogeneous surface structure: Locally and parallel to the trenches, the surface is very smooth with a root mean square roughness calculated parallel to the trenches (i. e. in y-direction in Figure 1) below 5 nm. Perpendicular to the trenches, all surfaces feature a nearly sinusoidal periodicity that results in a vigorously homogeneous surface and a high symmetry within its repetitive structuring. The wavelengths and amplitudes of the periodic structures are in the same size range as the dimensions of *S. aureus* cells, as sketched in Figure 1b. Therefore, the wrinkled PDMS surfaces are a well-suited substrate to determine the adhesion force of *S. aureus* cells at different locations on the cell wall by SCFS.

S. aureus shows periodic but not symmetrical adhesion patterns on wrinkled PDMS

To measure the adhesion of *S. aureus* cells at different positions relative to the periods of the wrinkled PDMS surfaces, the substrates were mounted such that the trenches on the surfaces were parallel to the y-direction of the AFM scan area. Correct positioning was verified by scanning the surface before performing SCFS experiments. (An inclination of up to 1° was accepted, otherwise the sample was repositioned.)

Then, several hundred force-distance curves were recorded with one and the same single cell while the x-position between each two consecutive curves was changed by a constant value (of 20-30 nm). From every curve, the adhesion force and the z-height at which the retraction began (termed “initial retraction height”) were determined, and the results are shown in Figure 2a for one exemplary cell.

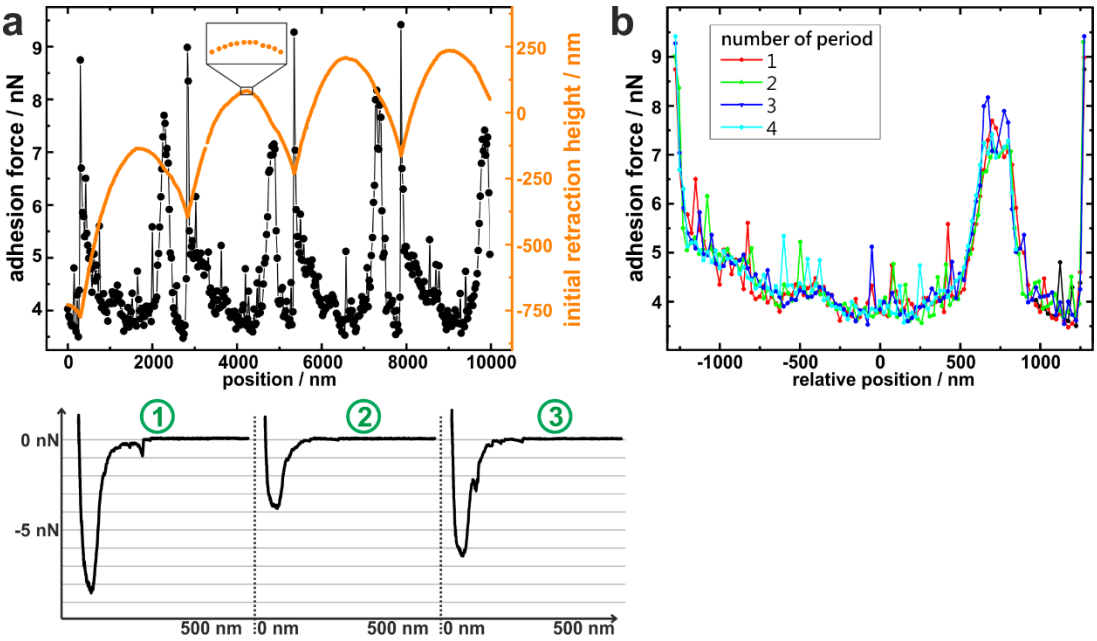

Fig. 2. Adhesion force as function of position on the wrinkled surface. Raw data for an exemplary *S. aureus* cell. a) Adhesion force (black dots) and height of the cantilever at which retraction started ("initial retraction height", orange line) for different positions on the surface. For three positions (1/2: at the minimum/maximum of the surface topography, 3: at an intermediate position with high adhesion), exemplary force-distance curves are shown. The zoom into the orange line highlights the quality of the initial retraction height data. b) Overlay of the adhesion force data from a) for each period of the surface (that was determined using retraction height data) in dependence of the distance from the maximum of each period.

The graph of the initial retraction heights (orange data in Fig. 2a) has a distinct periodicity which reflects the surface topography. Notably, it does not have the same curve form as the AFM scans in Figure 1d. The reason for this is that the AFM tip that scanned the surface had a tip radius of approximately 20 nm while the force-distance curves were recorded with an attached bacterial cell that features a much wider radius (approx. 500 nm). Hence, the cell – in contrast to the tip – cannot exactly follow the surface topography, especially not in the trenches of the surface (For an explanatory sketch, see Supplementary Materials Figure S1). In addition, the AFM has a certain vertical drift that causes a linear offset in the orange data in Figure 2a. Nevertheless, the data reproduce the surface periodicity very well and can be used to extract the position of each force-distance curve in relation to the periodic structures of the substrate.

All recorded force-distance curves (three of which are exemplary shown in Fig. 2a) have a similar cup-like shape, suggesting that a rather high number of cell wall molecules is responsible for adhesion on every position of the wrinkled PDMS (15).

Notably, the recorded adhesion forces show a periodicity with the same wavelength as the initial retraction heights: For example, the graph of the adhesion forces has local maxima at x = 200 nm, 2800 nm, 5200 nm, and 7800 nm, each of which nicely corresponds to a minimum in the initial retraction height data.

Next, the recorded adhesion forces were subdivided relative to the periodicity and plotted accordingly, as shown in Figure 2b. In this graph, the recorded adhesion forces for a given position are in the same range and show certain characteristics: For example, the forces are highest at the edges of the plots, corresponding to the trenches of the wrinkled surface. Figure 2 b also shows nicely that the adhesive force values are not symmetrically distributed within each period of surface ripple ($F_{adh}(x) \neq F_{adh}(-x)$), though the surface topography (reflected by the initial retraction heights) is highly symmetrical within each period. In other words, although the surface topography in each period is symmetrical, the adhesion forces measured on this topography are not. Hence on can assume the existence of areas with larger and smaller adhesive power on the cell's surface that will be characterized in more detail in the next section.

Experimentally tested cells show individual, asymmetric adhesion curves

In total, the adhesion at different positions within one period of the sinusoidal surface was investigated for 14 individual *S. aureus* cells as described in the previous paragraph. For every cell, the measured adhesion forces on corresponding positions of different periods of the surfaces (see Figure 3a) were used to calculate the mean adhesion force relative to the periodicity of the substrate. Figure 3b shows the mean adhesion forces of all cells in dependence of the relative position within one period of the surface topography, called adhesion profiles hereinafter. The beginning and end of the x-axes refer to the minima of the surface ("trenches") while the middle corresponds to the local maxima ("hills") as shown in Figure 3a.

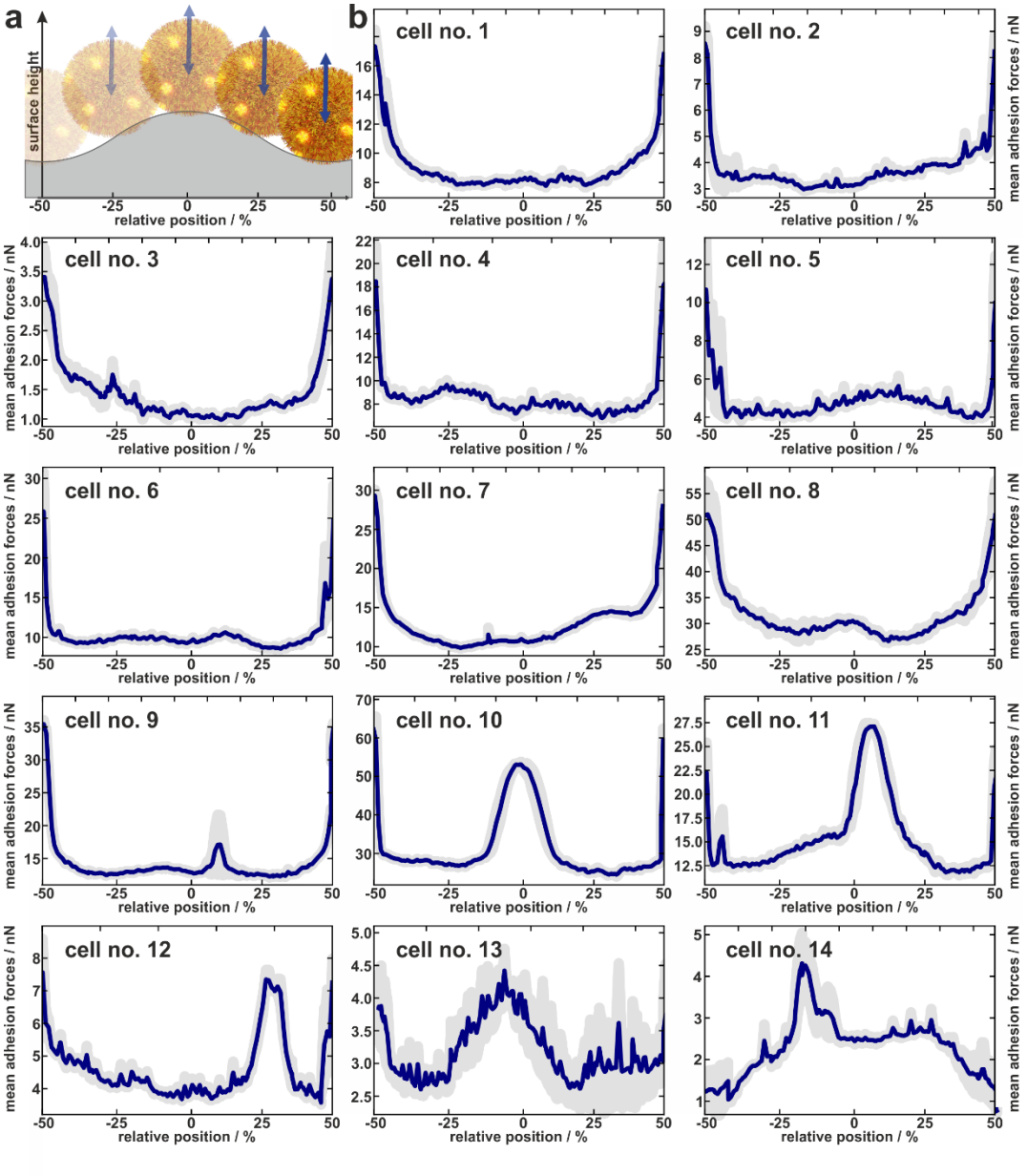

Fig. 3. Experimentally determined distribution of adhesion forces of 14 cells. a) About to scale sketch to illustrate how the x-positions fit to the relative position within one period of the surface. b) Mean adhesion forces (and error of the mean as shaded area) of 14 cells averaged over several periods of the wrinkled surface relative to the topographical maximum of the surface periods.

Cells no. 1-12 show comparatively high adhesion forces at the minima of the surface. This can be explained geometrically: Due to the similar curvatures of the two surfaces of the wrinkled substrate and the soft proteinaceous bacterial cell wall, they adapt to each other and thus the surface area that is accessible to the cell tethers increases (31, 32). Between these maxima, the mean adhesion forces are up to a factor of three smaller but feature local maxima that are more or less pronounced depending on the individual cell. For example, cell no. 1 shows a “bathtub-shaped” curve with only small local maxima. In contrast, other

cells, e. g. cell no. 10, feature very pronounced local maxima between the maxima of the curves.

Notably, the existence of local maxima or their relative size does not depend on the measured mean adhesion forces (i. e. the mean value of the measured adhesion forces on every position). In other words, cells with rather low overall adhesive strength can have distinct positions with relatively high adhesion (e. g. cell no. 13), while other cells with a rather strong overall adhesion do not show these positions (e. g. cell no. 6). The cells no. 13 and no. 14, for instance, even do not show the highest adhesion in the minima of the surface. Apparently, the adhesion strength of their highly adhesive positions on the cell wall surpasses the effect of increased contact area-enhanced stronger adhesion in the period's minima.

To summarize, the measured adhesion forces of the tested cells not only show often distinct local maxima in the surface minima, and their distribution within one period is not symmetrical. In order to analyze this effect, it is important to note that we do not necessarily measure the same adhesion forces on the wrinkled surface as we would on a flat substrate: Since the cantilever with the bacterial cell moves only in a vertical direction, the direction of the cell's movement relative to the local normal direction of the surface changes for different positions within one period. Since the mechanic properties of the involved macromolecules during elongation under different angles are not known, it is not straightforward to correct the measured values for this geometric effect and thus directly determine the distribution of adhesins on the cell wall. Therefore, we attempted to derive this distribution of adhesive molecules on the cell wall by comparing the experimentally measured data with theoretical simulations, as described in the next section.

Comparison to simulations

To unravel how the adhesion force profiles in Figure 3 could emerge from bacteria with differently distributed adhesive capability on their cell envelope, we simulated the bacteria as hard spheres on which adhesive molecules are distributed. Since the adhesion process of *S. aureus* is governed by the collective response of individual macromolecules to stretching (15, 16, 33), whose mechanical properties, e. g. length, and stiffness, are heterogenous and can lead to macroscopically nonlinear behavior in SCFS experiments (33), we used the model published by Maikranz et al. (15) and extended it with respect to the surfaces used in the SCFS experiments.

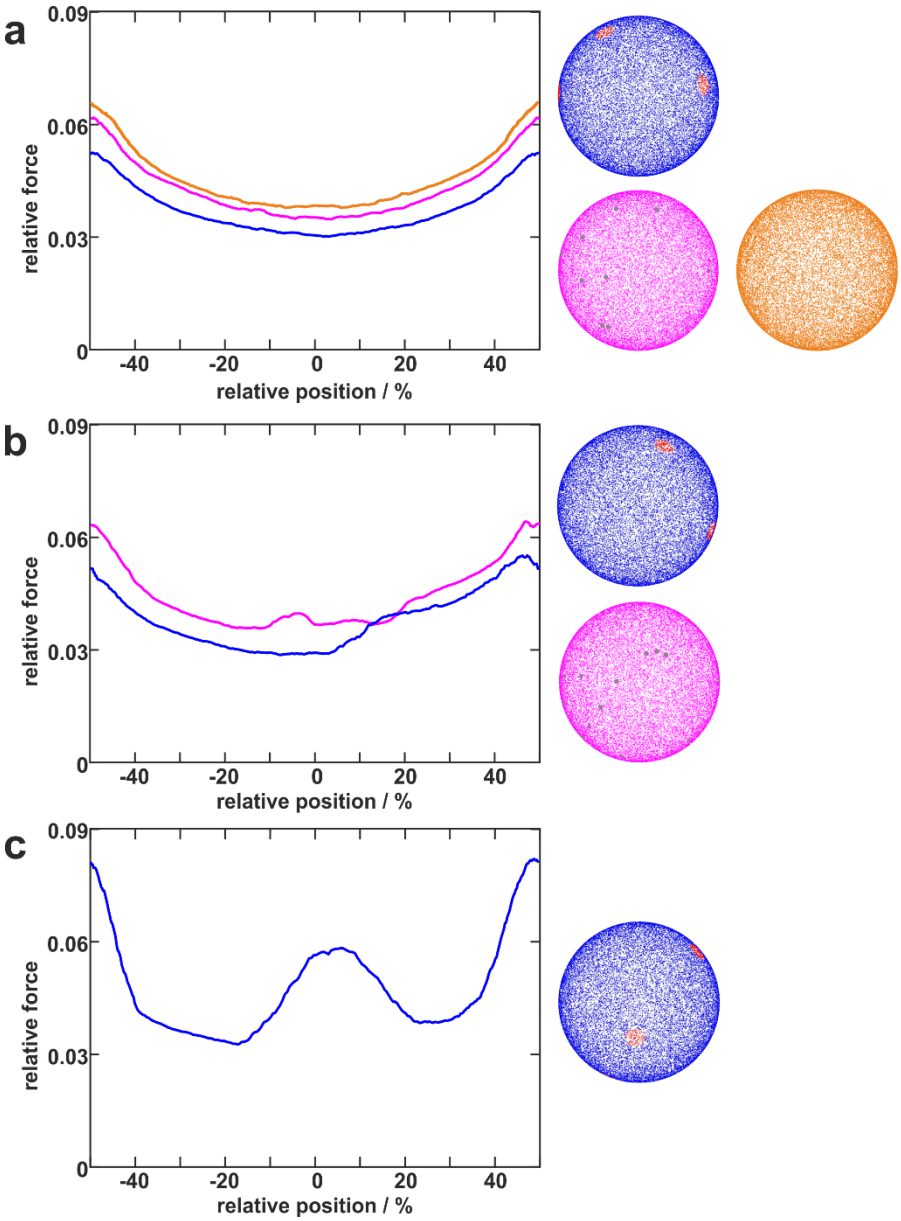

Fig. 4. Distribution of adhesive molecules and corresponding simulation results. Examples of simulated cells with differently distributed adhesive molecules (right) and corresponding adhesion force profiles (left). The blue cells with distinct large patches (red) with a certain distance to each other can reproduce several types of profiles (blue lines in a, b, c). In contrast, the pink cells having independently distributed small patches (grey) can only reproduce rather smooth curves (pink line in a) or curves with only small "humps" (pink lines in b). The orange cell with homogeneously distributed molecules can only reproduce smooth cup-shaped profiles (orange line in a).

This model provides a correct force scale but is computational very expensive. Because of the latter, we also used a rather simple geometric model, where adhesive molecules are modeled as rods of fixed length that protrude outward along the normal of the cell that is modeled as a hard sphere. After the cell is brought into tangential contact at position x above the surface, the relative adhesive strength is calculated from the molecules intersecting with

the surface (each molecule might also have a different adhesiveness, for details, see Materials and Methods and Supplementary Materials). Of note, the geometric model does not provide the correct force scale but relative values. A comparison of both models for a cell with homogeneously distributed macromolecules that adheres inside one period shows that although the geometric model produces smoother curves, the overall shapes and relative magnitudes of the curves from both models are the same (see Fig. S2). Therefore, the models seem suitable to analyze the experimental results. Since the mechanical model is computational expensive, we use the geometric model in the following to gain further insight.

In Figure 4, the resulting adhesion force profiles from different simulations with different parameters as well as a graphical representation of the simulated cells, for which the curves were calculated, are shown. Exemplary curves are chosen such that they are in good accordance to certain experimental curves in Figure 3.

From these data, several properties of the distribution of adhesion capability can be obtained: i) "Bathtub-shaped" smooth curves (as for example cell no. 1 in Fig. 3a) come from a rather high number (about 50.000) of homogeneously distributed molecules i. e. cells without patches or from cells with patches that do not reach the surface (as in Figure 4a).

Of note, the simulated adhesion force profiles (and also the ones from the full mechanical model, see Fig. S2 in the Supplementary Materials) are rather "cup-shaped" and do not display the fast drop of adhesion forces at the edges of the plot with rather constant values in between as observed in the experiments: In the model, the ratio of maximal to minimal force is not 2-3:1 as in the experiments but always lower 2:1. Hence, compared to the models, the experimentally tested cells show rather strong adhesion in the valleys as well as at the maxima of the surface. We cannot reveal the origin of this deviation between experiment and simulation. However, deformation of the PDMS substrates as the cell is approached and retracted along the surface normal (which is expected to be strongest in the in the minima and maxima of the sinusoidal surface) could explain the stronger forces measured.

ii) The experimental adhesion force profiles which deviate from a rather smooth bathtub-shape and display shoulders at the edges of the plot or "humps" in between come from bacterial cells that have adhesive patches in addition to a background of homogeneously distributed adhesive molecules. The simulations show that these patches can either be independently, randomly distributed and up to 30 in number (pink cells in Fig. 4) with 50 nm diameter or that they can be very distinct with a certain minimal distance to each

other and hence less numerous but larger (diameter of 250 nm). The patches themselves contain 15-50 homogeneously distributed adhesive molecules each.

Alternatively, the "fluctuations" and small "humps" in the profiles could come from a reduced overall density of adhesive molecules: The smaller the total amount of adhesive molecules, the more irregular are the profiles. If there are only about 100 molecules on the whole cell, profiles with strongly scattering values are obtained similar to the ones from cells number 13 and 14 in Figure 3 (see Fig. S4a).

iii) Adhesion force profiles that display a distinct "peak" between the two maxima at the plot edges must come from cells with distinct patches, which in turn also have a certain distance to each other. From the parameters of our simulations (see Materials and Methods), we can estimate the patch diameter of around 250 nm and their distance of about 850 nm. Inside the patches, the number of molecules or their individual adhesive strength are enhanced (by about a factor of 15, see also Fig. S3).

Hence, the main properties of the experimental results can be reproduced by the used geometric model in which the cells have a patchy distribution of adhesive molecules on their cell wall.

Discussion

We investigated the adhesion capability of *S. aureus* cells to a structured surface by single-cell force spectroscopy to measure how the strength of adhesion depends on the position relative to a structured surface. We found that the adhesion of bacteria is not only cell-specific (as shown before (15, 17)), but also depends on the position on the cell envelope. Simulations reproducing the experimental results gave information about the distribution of the adhesion capability on the cell wall: Our data show that *S. aureus* cells have highly adhesive patches on their cell wall. Depending on the probed cell, these patches can have different properties: While the experimental results for some cells can come from a rather high number (up to 30) of independent patches with diameters of about 50 nm, other cells must have fewer distinct patches (about 5-6 patches with a distance of about 850 nm) with a lager diameter of about 250 nm.

Hence, our results for coccal-shaped Gram-positive *S. aureus* cells nicely complement the patchy colloid model of adhesion for rod-shaped Gram-negative *E. coli* cells by Vissers *et al.* (27). Their experiments show that *E. coli* cells have distinct patches on their surface and that the number of these patches defines adhesive strength of a cell; if no patches exist, a cell hardly adheres. However, our results - together with former studies - lead to a slightly

different notion for Gram-positive *S. aureus* cells: Since the force-distance curves on all positions of the surface look similar, namely cup-shaped, *S. aureus* cells seem to have many adhesive molecules at almost every position of the cell wall, but the strength of adhesion has maxima at certain locations (15).

At these points, not necessarily the number of molecules is maximal, but rather their individual properties lead to maximum adhesive strength (17). Although we do not determine the origin of the adhesive patches, they seem to have similar properties as the clusters of certain proteins at the cell wall: For example, the simulated patchy spheres in Figure 4 are quite similar to the electron micrographs showing the distribution of protein A and Clumping factor A in the publication of Harris *et al.* (21). Another candidate for the origin of the adhesive patches might be Cna since it also clusters in nanometer-sized domains on the *S. aureus* cell wall (25). However, we cannot answer the question, whether the adhesive patches are "hot spots" where many adhesins occur together, whether there are several clusters, each containing only one type of adhesin, or whether the combination of different adhesive molecules with certain mechanical properties renders a given position at the cell wall highly adhesive.

Moreover, we cannot resolve if cells that do not show very distinct maxima in the adhesion curves (for example cell no. 1 in Figure 3) do not have any patches, or if – by chance – none of the patches come in contact to the surface. Along this line, it might be possible that only one half of the cell, for example the part that was newly synthesized during cell division, has patches of high adhesion capability (34, 35). This might be exciting subject for further studies, in which adhesion measurements on structured surfaces could be combined with fluorescent labelling techniques (36). In that way, it will be possible to correlate the prevalence of certain proteins and/or former division planes with the adhesion capability of the investigated cells. Alternatively or in addition to this, extracellular vesicles formed and temporary retained on the *S. aureus* cell surface might contribute to this phenomenon (37, 38).

Our findings have consequences for science and material development: In future experiments and especially when designing models for simulations, the cells should not be regarded as rather uniform colloids, but as objects with as heterogeneous surface properties. Finally, these differences in adhesive properties should be considered in the design of new antibacterial materials for the reduction of infections.

Materials and Methods

Production of the Wrinkled Surfaces: PDMS was prepared by mixing the pre-polymer and curing agent of a Dow Corning Sylgard 184 PDMS Kit in 5:1 ratio, curing it at RT for 24 h followed by a thermal treatment of 4 h at 80 °C under ambient conditions. Slabs of 4.5 cm × 1.0 cm were cut out, cleaned with Milli-Q water and dried with nitrogen. The slabs were clamped in a custom-made stretching-device and strained uniaxially to 5–10 % of their initial length. Afterwards the slabs were placed in a low-pressure RF-plasma chamber and treated for 120–300 s with a H_2-plasma at 800 W. Eventually the pre-strain is released, revealing opaque colored wrinkles on the PDMS topside (28).

Bacterial Cultures: *S. aureus* cells, strain SA113, from a deep-frozen stock culture were plated on blood agar for one day and a fresh plate was used no longer than a week. The day before the experiments, one colony from the plate was transferred into 5 ml of tryptic soy broth (TSB) and cultured for 16 h at 37 °C under agitation (150 rpm). To get cells in exponential growth phase, at the day of the experiments, 40 µl of the overnight culture were transferred into 4 ml of fresh TSB and cultured for 2.5 h at 37 °C under agitation (150 rpm). From this final culture, 1 ml was washed three times with sterile phosphate buffered saline (TSB) at an acceleration of 40,000 g. The cells in PBS were stored at 4 °C and used no longer than 6 h.

Single-Cell Force Spectroscopy: As described in the publication of Thewes *et al.*, using a micromanipulator (Narishige Group, Tokyo, Japan), single bacterial cells were immobilized on tipless cantilevers (MLCT-0-F with nominal spring constants of 0.03 N/m from Bruker, Santa Barbara), which were beforehand coated with polydopamine (39). With these bacterial probes, single-cell force spectroscopy measurements were performed using a Bioscope Catalyst (Bruker) at room temperature in PBS (pH 7.3, ionic strength 0.1728 mol/l). Force-distance curves were performed with a ramp size of 800 nm and a velocity of 800 nm/s. The force trigger, i. e. the maximal force with which the cell is pressed onto the substrate prior to immediate retraction, was set to 300 pN. With every cell, some hundreds (between 400 and 500) of consecutive curves were recorded in a straight line with a constant lateral distance (of 20 nm, 25 nm, or 30 nm; called x-offset hereinafter) between consecutive curves on one of the three PDMS samples. Hence, force measurements on 4–5 equivalent positions in different periods were recorded. No systematic change in the adhesion behavior, such as a decreasing adhesive strength due to cell fatigue, could be observed even after 500 curves. The direction of this straight line was perpendicular to the trenches in the wrinkled PDMS samples with a deviation of less than 1°. For every probed cell, the parameters of the

experiment (number of curves, x-offset, underlaying PDMS sample) are given in Table S1 in the Supplementary Materials.

Analysis: From every recorded force-distance curve, a baseline was first subtracted, and the adhesion force was determined as the minimum force that occurred during retraction of the cantilever. In addition, the z-position of the instrument's height sensor at the beginning of the retraction was recorded, and also corrected for a linear baseline shift caused by a drift of the AFM piezo. The adhesion forces and the positions where the retraction of the cantilever started were plotted against the corresponding x-offset and the periodicity was determined automatically as follows: The curves of the initial retraction heights were searched for peaks in negative direction (denoting the valleys of the surface). The positions of these peaks were used to divide the calculated adhesion forces into sections that correspond to the different periods of the surface. Since the wavelength of the periodicity can locally vary and since it does not necessarily fit a multiple of the x-offset, the data for each period were slightly shifted in x-direction, so that each period has the same size.

Simulations: To obtain an estimate of the distribution of adhesive molecules on the bacterial cell wall, we used two types of models:

Monte Carlo Model – **Thermally Fluctuating Macromolecules:** Since the used substrate surface is not flat**,** and therefore geometric constraints of the surface-sphere geometry non-uniformly affect the interactions of the macromolecules along the substrate, we extended the model of Maikranz et al. (15), in which the bacterium is modeled as a hard sphere, decorated with $N = 50.000$ thermally fluctuating macromolecules, for whose mechanical response of a WLC polymer model with probabilistic parameters is used. In the extension, we consider thermal length fluctuations of each macromolecule along its respective normal, and mechanical stretching, and therefore acting force on the sphere, if the macromolecule is bound to the substrate (for model details, see Supplementary Materials).

Geometric Model: For the bacterium, a hard sphere with a radius of 500 nm was used. Adhesive molecules in the cell envelope, were modeled as rods of constant lengths protruding from the surface of the cell outwards in normal direction. The model provides the relative adhesion force f of the cell at point x along the sinusoidal surface (amplitude $A = 190$ nm, wavelength $\lambda = 2750$ nm) by a weighted count of all rods intersecting the sine surface in relation to the total number of rods (for details, see Supplementary Materials). We investigated homogeneous as well as patchy distributions of adhesive capabilities as described below.

A random, homogeneous distribution of rods on the cell surface was realized by placing rods with weight one randomly on the sphere (independently and uniformly distributed). To obtain complete spatial randomness the number N of rods follows a Poisson distribution (40). Adhesive patches have been produced by placing clusters of fixed radial extension (spherical caps) onto a homogeneous distribution. Inside these clusters the adhesiveness was increases by either placing additional rods inside the cluster or by giving all rods inside a cluster a higher adhesive weight. These clusters have been realized in two different ways: i) Clusters via random position: A Poisson distributed number of spherical caps with constant radii (125 nm) were placed at random positions. Note that different clusters might overlap. ii) Clusters via random sequential adsorption (RSA), for example, see (41): In each adsorption step, a spherical cap with constant radius (125 nm) and a constant "radius of repulsion" (850 nm) was randomly positioned on the spheres surface. The position of the following spherical caps was only accepted if their "radii of repulsion" did not overlap with previously placed caps. The RSA process was stopped after 1000 runs, i. e. when with a high probability no additional spherical caps could be added

References

1. Thomas Bjarnsholt. The role of bacterial biofilms in chronic infections. *Apmis*, 121:1–58, 2013.
2. Luanne Hall-Stoodley, J William Costerton, and Paul Stoodley. Bacterial biofilms: from the natural environment to infectious diseases. *Nature Reviews Microbiology*, 2(2):95–108, 2004.
3. Ki Soo Park, Chen-Han Huang, Kyungheon Lee, Yeong-Eun Yoo, Cesar M Castro, Ralph Weissleder, and Hakho Lee. Rapid identification of health care–associated infections with an integrated fluorescence anisotropy system. *Science Advances*, 2(5):e1600300, 2016.
4. Cindy M Liu, Lance B Price, Bruce A Hungate, Alison G Abraham, Lisbeth A Larsen, Kaare Christensen, Marc Stegger, Robert Skov, and Paal Skytt Andersen. Staphylococcus aureus and the ecology of the nasal microbiome. *Science Advances*, 1(5):e1400216, 2015.
5. Daniela Berger, Aviva Rakhamimova, Andrew Pollack, and Zvi Loewy. Oral biofilms: development, control, and analysis. *High-Throughput*, 7(3):24, 2018.
6. Carla Renata Arciola, Davide Campoccia, and Lucio Montanaro. Implant infections: adhesion, biofilm formation and immune evasion. *Nature Reviews Microbiology*, 16(7):397, 2018.
7. Eloise D Austin, Sean B Sullivan, Susan Whittier, Franklin D Lowy, and Anne-Catrin Uhlemann. Peripheral intravenous catheter placement is an underrecognized source of staphylococcus aureus bloodstream infection. In *Open Forum Infectious Diseases*, volume 3, page ofw072. Oxford University Press, 2016.
8. Mitchell D Feldman, Amy J Petersen, Leah S Karliner, and Jeffrey A Tice. Who is responsible for evaluating the safety and effectiveness of medical devices? the role

of independent technology assessment. *Journal of General Internal Medicine*, 23(1):57–63, 2008.

9. Aaron J Tande and Robin Patel. Prosthetic joint infection. *Clinical Microbiology Reviews*, 27(2):302–345, 2014.
10. Franklin D Lowy. Staphylococcus aureus infections. *New England Journal of Medicine*, 339(8):520–532, 1998.
11. Maneesha K Suresh, Raja Biswas, and Lalitha Biswas. An update on recent developments in the prevention and treatment of staphylococcus aureus biofilms. *International Journal of Medical Microbiology*, 309(1):1–12, 2019.
12. Niels Høiby, Thomas Bjarnsholt, Michael Givskov, Søren Molin, and Oana Ciofu. Antibiotic resistance of bacterial biofilms. *International Journal of Antimicrobial Agents*, 35(4):322–332, 2010.
13. Hans-Curt Flemming and Jost Wingender. The biofilm matrix. *Nature Reviews Microbiology*, 8(9):623–633, 2010.
14. Steven YC Tong, Joshua S Davis, Emily Eichenberger, Thomas L Holland, and Vance G Fowler. Staphylococcus aureus infections: epidemiology, pathophysiology, clinical manifestations, and management. *Clinical Microbiology Reviews*, 28(3):603–661, 2015.
15. Erik Maikranz, Christian Spengler, Nicolas Thewes, Alexander Thewes, Friederike Nolle, Philipp Jung, Markus Bischoff, Ludger Santen, and Karin Jacobs. Different binding mechanisms of staphylococcus aureus to hydrophobic and hydrophilic surfaces. *Nanoscale*, 12(37):19267–19275, 2020.
16. Nicolas Thewes, Alexander Thewes, Peter Loskill, Henrik Peisker, Markus Bischoff, Mathias Herrmann, Ludger Santen, and Karin Jacobs. Stochastic binding of staphylococcus aureus to hydrophobic surfaces. *Soft Matter*, 11:8913–8919, 2015.
17. Christian Spengler, Nicolas Thewes, Philipp Jung, Markus Bischoff, and Karin Jacobs. Determination of the nano-scaled contact area of staphylococcal cells. *Nanoscale*, 9:10084–10093, 2017.
18. Christian Spengler, Friederike Nolle, Johannes Mischo, Thomas Faidt, Samuel Grandthyll, Nicolas Thewes, Marcus Koch, Frank Müller, Markus Bischoff, Michael Andreas Klatt, et al. Strength of bacterial adhesion on nanostructured surfaces quantified by substrate morphometry. *Nanoscale*, 11(42):19713–19722, 2019.
19. Olaf Schneewind and Dominique M Missiakas. Staphylococcal protein secretion and envelope assembly. *Gram-Positive Pathogens*, pages 592–598, 2019.
20. Andrea C DeDent, Molly McAdow, and Olaf Schneewind. Distribution of protein a on the surface of staphylococcus aureus. *Journal of Bacteriology*, 189(12):4473–4484, 2007.
21. Llinos G Harris, SJ Foster, Robert G Richards, et al. An introduction to staphylococcus aureus, and techniques for identifying and quantifying s. aureus adhesins in relation to adhesion to biomaterials: review. *Eur Cell Mater*, 4(3):100–20, 2002.
22. Pauline Vitry, Claire Valotteau, Cécile Feuillie, Simon Bernard, David Alsteens, Joan A Geoghegan, and Yves F Dufrêne. Force-induced strengthening of the interaction between staphylococcus aureus clumping factor b and loricrin. *MBio*, 8(6), 2017.
23. Philippe Herman-Bausier, Cristina Labate, Aisling M Towell, Sylvie Derclaye, Joan A Geoghegan, and Yves F Dufrêne. Staphylococcus aureus clumping factor a

is a force-sensitive molecular switch that activates bacterial adhesion. *Proceedings of the National Academy of Sciences*, 115(21):5564–5569, 2018.

24. Philippe Herman-Bausier, Sofiane El-Kirat-Chatel, Timothy J Foster, Joan A Geoghegan, and Yves F Dufrêne. Staphylococcus aureus fibronectin-binding protein a mediates cell-cell adhesion through low-affinity homophilic bonds. *MBio*, 6(3):e00413–15, 2015.
25. Philippe Herman-Bausier, Claire Valotteau, Giampiero Pietrocola, Simonetta Rindi, David Alsteens, Timothy J Foster, Pietro Speziale, and Yves F Dufrêne. Mechanical strength and inhibition of the staphylococcus aureus collagen-binding protein cna. *MBio*, 7(5), 2016.
26. Philippe Herman, Sofiane El-Kirat-Chatel, Audrey Beaussart, Joan A Geoghegan, Timothy J Foster, and Yves F Dufrêne. The binding force of the staphylococcal adhesin sdrg is remarkably strong. *Molecular Microbiology*, 93(2):356–368, 2014.
27. Teun Vissers, Aidan T Brown, Nick Koumakis, Angela Dawson, Michiel Hermes, Jana Schwarz-Linek, Andrew B Schofield, Joseph M French, Vasileios Koutsos, Jochen Arlt, et al. Bacteria as living patchy colloids: Phenotypic heterogeneity in surface adhesion. *Science Advances*, 4(4):eaao1170, 2018.
28. Bernhard Alexander Glatz and Andreas Fery. The influence of plasma treatment on the elasticity of the in situ oxidized gradient layer in pdms: towards crack-free wrinkling. *Soft Matter*, 15(1):65–72, 2019.
29. Alexandra Schweikart and Andreas Fery. Controlled wrinkling as a novel method ffor the fabrication of patterned surfaces. *Microchimica Acta*, 165(3-4):249–263, 2009.
30. Ye Yu, Charlene Ng, Tobias AF Koönig, and Andreas Fery. Tackling the scalability challenge in plasmonics by wrinkle-assisted colloidal self-assembly. *Langmuir*, 35(26):8629–8645, 2019.
31. Ralf Helbig, Denise Günther, Jens Friedrichs, Florian Rößler, Andrés Lasagni, and Carsten Werner. The impact of structure dimensions on initial bacterial adhesion. *Biomaterials Science*, 4(7):1074–1078, 2016.
32. Allon I Hochbaum and Joanna Aizenberg. Bacteria pattern spontaneously on periodic nanostructure arrays. *Nano Letters*, 10(9):3717–3721, 2010.
33. Sassan Ostvar and Brian D Wood. Multiscale model describing bacterial adhesion and detachment. *Langmuir*, 32(20):5213–5222, 2016.
34. Robert D Turner, Emma C Ratcliffe, Richard Wheeler, Ramin Golestanian, Jamie K Hobbs, and Simon J Foster. Peptidoglycan architecture can specify division planes in staphylococcus aureus. *Nature Communications*, 1(1):1–9, 2010.
35. Richard Wheeler, Stéphane Mesnage, Ivo G Boneca, Jamie K Hobbs, and Simon J Foster. Super-resolution microscopy reveals cell wall dynamics and peptidoglycan architecture in ovococcal bacteria. *Molecular Microbiology*, 82(5):1096–1109, 2011.
36. Bruno M Saraiva, Moritz Sorg, Ana R Pereira, Mário J Ferreira, Léo C Caulat, Nathalie T Reichmann, and Mariana G Pinho. Reassessment of the distinctive geometry of staphylococcus aureus cell division. *Nature communications*, 11(1):1–7, 2020.
37. Eun-Young Lee, Do-Young Choi, Dae-Kyum Kim, Jung-Wook Kim, Jung Ok Park, Sungjee Kim, Sang-Hyun Kim, Dominic M Desiderio, Yoon-Keun Kim, Kwang-Pyo Kim, et al. Gram-positive bacteria produce membrane vesicles: proteomics-based characterization of staphylococcus aureus-derived membrane vesicles. *Proteomics*, 9(24):5425–5436, 2009.

38. Hansol Im, Sujin Lee, Steven A Soper, and Robert J Mitchell. Staphylococcus aureus extracellular vesicles (evs): surface-binding antagonists of biofilm formation. *Molecular BioSystems*, 13(12):2704–2714, 2017.
39. Nicolas Thewes, Peter Loskill, Christian Spengler, Sebastian Hümbert, Markus Bischoff, and Karin Jacobs. A detailed guideline for the fabrication of single bacterial probes used for atomic force spectroscopy. *The European Physical Journal E*, 38(12):140, 2015.
40. Günter Last and Mathew Penrose. *Lectures on the Poisson process*, volume 7. Cambridge University Press, 2017.
41. Sung Nok Chiu, Dietrich Stoyan, Wilfrid S Kendall, and Joseph Mecke. *Stochastic geometry and its applications*. John Wiley & Sons, 2013.

Acknowledgments

Funding: The authors thank the German Research Foundation (DFG) for funding within the context of the Collaborative Research Center SFB 1027 (projects B1 and B2). C. S. acknowledges funding from the DFG the project JA 905/6. M. A. K. acknowledges funding by the Princeton University Innovation Fund for New Ideas in the Natural Sciences. A. F. and B. G. acknowledge funding from the DFG project number FE 600/20-1. K. J. acknowledges funding within the Max Planck School Matter to Life supported by the German Federal Ministry of Education and Research (BMBF) in collaboration with the Max Planck Society.

Author contributions: C. S. designed the study, performed AFM experiments, analyzed the data and wrote the manuscript. B. A. G. produced the wrinkled surfaces, discussed the results and helped writing the manuscript. E. M. designed the model of thermally fluctuating macromolecules and performed the simulations, analyzed the data, discussed the results and wrote the manuscript. M. B. supervised the study and discussed the results. M. A. K. designed the geometric model and performed the simulations, analyzed the data, discussed the results. L. S. designed and supervised the study and discussed the results. A. F. supervised the study and helped writing the manuscript. K. J. designed and supervised the study, discussed the results and helped writing the manuscript.

Competing interests: There are no conflicts of interest to declare.

Data and materials availability: The raw data can be provided on reasonable request.